ACS SyntheticBiology

Research Article

pubs.acs.org/synthbio

Engineering Bacterial Microcompartment Shells: Chimeric Shell Proteins and Chimeric Carboxysome Shells

Fei Cai,[†,§] Markus Sutter,[§,∥] Susan L. Bernstein,[†,§] James N. Kinney,[§] and Cheryl A. Kerfeld*[,†,‡,§,∥]

[†]Department of Plant and Microbial Biology, [‡]Synthetic Biology Institute, University of California, Berkeley, California 94720, United States

[§]Physical Biosciences Division, Lawrence Berkeley National Laboratory, Berkeley, California 94720, United States

[∥]MSU-DOE Plant Research Laboratory, Michigan State University, East Lansing, Michigan 48824, United States

Supporting Information

ABSTRACT: Bacterial microcompartments (BMCs) are self-assembling organelles composed entirely of protein. Depending on the enzymes they encapsulate, BMCs function in either inorganic carbon fixation (carboxysomes) or organic carbon utilization (metabolosomes). The hallmark feature of all BMCs is a selectively permeable shell formed by multiple paralogous proteins, each proposed to confer specific flux characteristics. Gene clusters encoding diverse BMCs are distributed broadly across bacterial phyla, providing a rich variety of building blocks with a predicted range of permeability properties. In theory, shell permeability can be engineered by modifying residues flanking the pores (symmetry axes) of hexameric shell proteins or by combining shell proteins from different types of BMCs into chimeric shells. We undertook both approaches to altering shell properties using the carboxysome as a model system. There are two types of carboxysomes, α and β. In both, the predominant shell protein(s) contain a single copy of the BMC domain (pfam00936), but they are significantly different in primary structure. Indeed, phylogenetic analysis shows that the two types of carboxysome shell proteins are more similar to their counterparts in metabolosomes than to each other. We solved high resolution crystal structures of the major shell proteins, CsoS1 and CcmK2, and the presumed minor shell protein CcmK4, representing both types of cyanobacterial carboxysomes and then tested the interchangeability. The *in vivo* study presented here confirms that both engineering pores to mimic those of other shell proteins and the construction of chimeric shells is feasible.

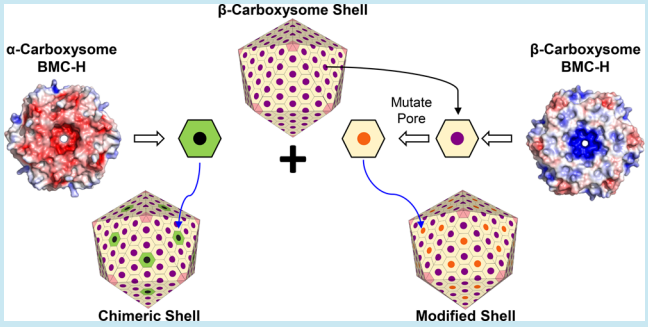

KEYWORDS: *bacterial microcompartment, self-assembly, chimeric protein shell, synthetic shell, metabolosome, cyanobacteria*

In the past decade, developments in bacterial cell biology have dramatically changed the traditional perspective on prokaryotic subcellular organization, leading to new strategies for microbial bioengineering. It is now clear that the bacterial cell is a highly ordered, dynamic system with counterparts to the eukaryotic cytoskeletal networks, signaling pathways, and organelles. The Bacterial Microcompartment (BMC), one of the best studied examples of a bacterial organelle, is distinctive as a protein-delimited organelle that sequesters enzymatic reactions to enhance rates or mitigate toxicity. The apparently icosahedral shell of the BMC is assembled from three types of building blocks: proteins containing one or two bacterial microcompartment (Pfam00936) domain(s) (referred as BMC-H and BMC-T, respectively) and proteins containing the Pfam03319 domain (referred as BMC-P).[1−7] Co-occurrence of genes encoding Pfam00936 and Pfam03319 domains in bacterial genomes has therefore been used for bioinformatic prediction of the potential to form BMCs.[8−10] As of January 2014, 2979 of 14765 publicly available microbial genomes among 16 phyla contain at least one BMC locus (surveyed in the Integrated Microbial Genomes database, http://img.jgi.doe.gov).

Three types of BMCs have been extensively characterized: the carboxysome for CO_2 fixation and the PDU and EUT metabolosomes for the breakdown of 1,2-propane-diol and ethanolamine, respectively. Recently, two bioinformatically identified BMC loci have been functionally characterized[11,12]. Although the functions of most BMCs await experimental studies, their tremendous potential as self-assembling organelles for applications in synthetic biology has made them a subject of recent intense research interest, particularly for the design and engineering of selectively permeable nanoreactors for cells.[9,13−24]

Among experimentally characterized BMCs, the carboxysome is uniquely involved in anabolic metabolism. Carboxysomes encapsulate the CO_2-fixing enzyme D-ribulose-1,5-bisphosphate carboxylase/oxygenase (RuBisCO) with carbonic anhydrase. They are found in all cyanobacteria and in some chemoautotrophic bacteria. There are two distinct carboxysome

Received: March 28, 2014
Published: August 12, 2014

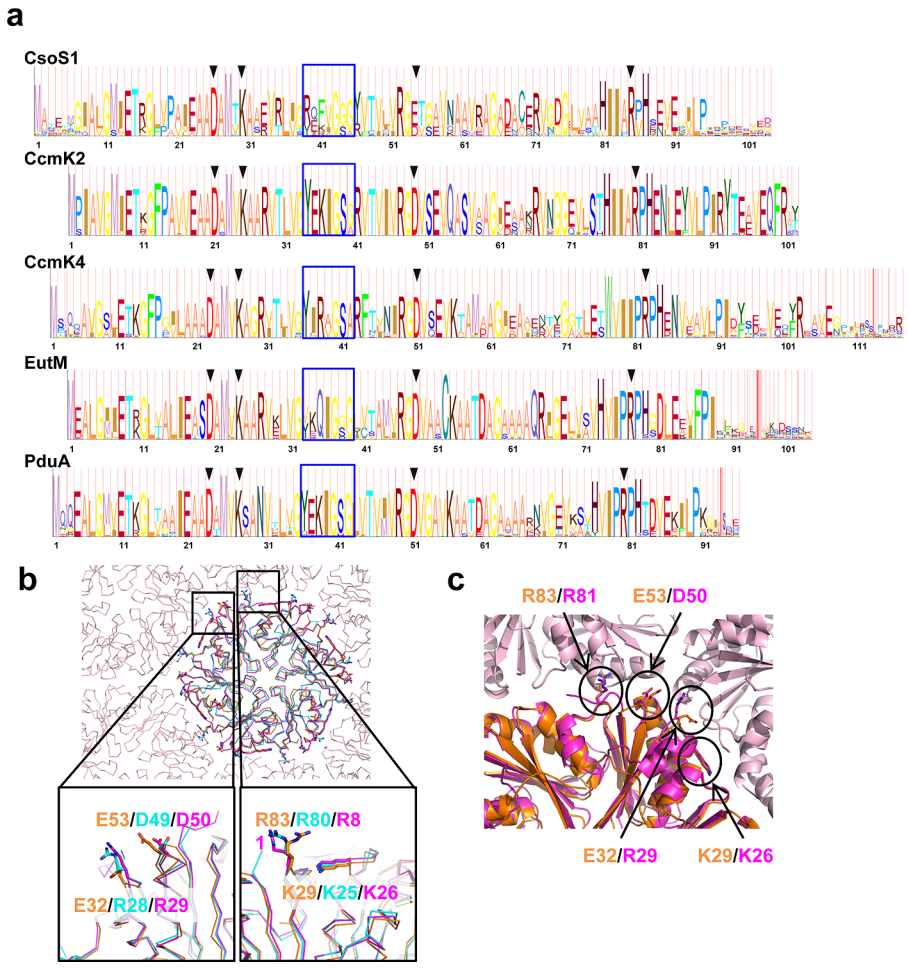

Figure 1. α- and β-carboxysome BMC-H proteins share several key residues that form the hexamer−hexamer interface. (a) Hidden Markov model (HMM) sequence logos for α- and β- carboxysome BMC-H proteins characterized in this study (CsoS1, CcmK2, and CcmK4) and representatives of the major shell proteins from the PDU and EUT metabolosomes (EutM and PduA from the ethanolamine and 1,2-propanediol utilization metabolosomes, respectively). A blue box outlines the residues surrounding the pores, and black triangles mark residues located at the two- or 3-fold interface of BMC-H hexamers in facets composed of these structures. Prepared with MUSCLE,[47] HMMER 3.0,[48] and LogoMat-M.[49] (b) Superposition of *Syn7942* CcmK2, *Syn7942* CcmK4, and *Pro9313* CsoS1 hexamer structures determined in this study, highlighting specific residues found at the two- and 3-fold interhexamer interface in a layer of hexamers. The tightly packed CcmK4 sheet is observed in the crystal packing (orange, CsoS1; cyan, CcmK2; magenta, CcmK4 center hexamer and light magenta for surrounding CcmK4 hexamers). (c) Close-up view of the α/β chimeric carboxysome shell model in which one hexamer of the CcmK4 sheet is replaced by a CsoS1 hexamer.

types, *cso* (α) and *ccm* (β), based on the form of RuBisCO and associated encapsulated proteins and gene organization. The carboxysome shell provided the first structurally characterized examples of BMC-H, BMC-T, and BMC-P proteins[1,2,4,5]. The structural studies led to a schematic model of the carboxysome shell, which is presumed to apply to other types of BMCs: hexamers containing a small central pore (4−7 Å) formed by BMC-H proteins (CsoS1 and CcmK for α- and β- types, respectively) tile together to form the facets of an icosahedral shell;[1,6] BMC-P proteins (CsoS4 and CcmL for α- and β- types, respectively) self-assemble into pentamers to cap the vertices.[5] Structural analysis together with biochemical evidence suggest that the facets also contain a stacked dimer of BMC-T trimers (CsoS1D and CcmP in α- and β-carboxysomes, respectively).[2,4,25]

Typically, BMC gene clusters contain multiple paralogs of BMC-H proteins; because they are structurally equivalent, this redundancy of hexameric shell proteins presumably reflects functional differences. The permeability properties of BMC-H paralogs are thought to be dictated by the conserved residues that flank the central pore of the BMC-H hexamers[1] (Figure 1a). In carboxysomes, BMC-H proteins are encoded by the *csoS1* and *ccmK* genes for α- and β-type carboxysomes, respectively. While *csoS1* genes are organized in the *cso*-operon, *ccmK* genes are arranged in multiple *ccm*-loci, including a core *ccm* operon (*ccmK-L-M-N-O*) and typically one or more satellite loci (e.g. *ccmK3-K4*); these seem to be regulated differently.[26−28] In *Synechococcus elongatus* PCC 7942 (*Syn7942*) there are three BMC-H paralogs, namely *ccmK2*, *ccmK3*, and *ccmK4*. Disruption of the *ccmK2* gene either by insertion or deletion, but not *ccmK3* and *ccmK4*, results in a carboxysome-less phenotype requiring high-CO_2 concentrations to survive.[29,30] This strongly suggests that regulation and expression of *ccmK2* are essential to the formation and function of the carboxysome.

Despite allowing the passage of the same metabolites (D-ribulose-1,5-bisphosphate, bicarbonate, and 3-phosphoglycerate), the shell proteins of the α- and β-carboxysomes are distinctly different. Based on their primary structures, CsoS1 and CcmK clearly fall into different clades on a phylogram

dx.doi.org/10.1021/sb500226j | *ACS Synth. Biol.* 2015, 4, 444−453

(Figure 2). The CsoS1 BMC-H protein of *Prochlorococcus marinus* str. MIT9313 (*Pro9313*) shares only 44% similarity to

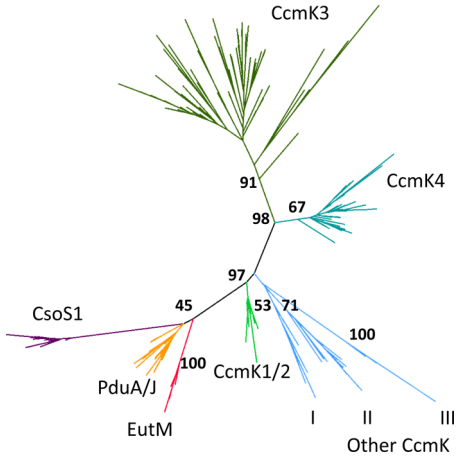

Figure 2. Phylogenetic tree for carboxysomal BMC-H proteins. BMC-H proteins from cyanobacterial α-carboxysome (Cso1, purple), β-carboxysomes (CcmK1/2, CcmK3, CcmK4, and other CcmKs, branches in green, dark green, cyan, and blue, respectively), PDU metabolosome (PduA/J, branches in orange), and EUT metabolosome (EutM, branches in red) are shown in an unrooted distance tree. Bootstrap values were obtained from 100 replicates. Numbers above the main branches indicate bootstrap values, and only branches receiving bootstrap values greater than 45 are represented.

CcmK2 of *Syn7942*. It is more closely related to the predominant shell proteins of catabolic metabolosomes, for example EutM (54% similarity)[31,32] and PduA (60% similarity),[33−35] the essential shell proteins of ethanolamine and 1,2-propanediol utilization metabolosome, respectively (Table 1 and Figure 2). Moreover, the residues flanking the

Table 1. Pairwise Alignment Matrix of BMC-H Proteins Studied in This Work and Two Representatives from Other Metabolosomes[a]

% identity/ similarity	*Pro9313* CsoS1	*Syn7942* CcmK2	*Syn7942* CcmK3	*Syn7942* CcmK4	EutM
Syn7942 CcmK2	40/44				
Syn7942 CcmK3	23/25	47/54			
Syn7942 CcmK4	27/30	46/53	50/58		
EutM	47/54	43/47	33/38	31/35	
PduA	53/60	53/58	32/39	37/43	63/66

[a]Pairwise sequence comparisons were done with online program EMBOSS-Needle (www.ebi.ac.uk/Tools/psa/emboss_needle) using default settings for gap penalty and matrix PAM30.

pore of CcmK2 are more similar to those of EutM and PduA than to the α-carboxysome CsoS1 pore residues (Figure 1a); however, it is assumed that the EUT and PDU shells are permeable to distinctly different metabolites (including ethanolamine, 1,2-propane-diol, propionate/propionyl phosphate). This could indicate that conserved pore residues may have an alternative or additional role shared by different types of BMCs.

Critical to the development of BMCs for bioengineering applications is the control of the selective permeability of the shell. Here, we report three new high resolution crystal structures of α- and β-carboxysome shell proteins, including the first evidence that shell facets could be composed entirely of CcmK4. Using these structures and the cyanobacterial carboxysome as a case study, we demonstrate that BMC-H pore residues can be interchanged among paralogs without abrogating shell formation, thereby presumably altering shell permeability. Finally, we show that it is feasible to construct α/β chimeric carboxysome shells, suggesting that mixing shell proteins from different BMC loci is a tractable approach to constructing shells with specific properties.

RESULTS AND DISCUSSION

A phylogenetic comparison of the shell proteins from the most extensively characterized BMCs, the α- and β-carboxysome and the PDU and EUT metabolosomes, shows that the BMC-H shell proteins of the two types of carboxysomes are significantly different and more closely related to major PDU and EUT BMC-H proteins than to each other (Figure 2). Moreover, the β-carboxysome paralogs also group into distinct clades. Sequence analysis of the carboxysome BMC-H proteins, PduA/J and EutM, indicates that the pore residues are also remarkably similar among CcmK2, PduA, and EutM but distinctly different from those of CcmK4 and CsoS1 (Figure 1a). Accordingly, we investigated the impact of interchanging paralog-specific pore residues (resulting in chimeric shell proteins) on shell formation and tested the potential for producing chimeric shells by mixing shell proteins from both α- and β-carboxysomes. Cyanobacterial carboxysomes are ideal for experiments in constructing chimeric shells because as a model system they provide a readout of both structural (visible in TEM or fluorescence microscopy) and functional complementarity; functionally impaired carboxysomes result in a distinctive high CO_2-requiring (*hcr*) phenotype. Because there was no structural data for BMC-H proteins from the cyanobacterial α-carboxysome nor from *Syn7942*, the model organism for β-carboxysome function and assembly studies,[30,36] we solved high resolution crystal structures of multiple BMC-H proteins from *Pro9313* and *Syn7942*. We subsequently used *Syn7942* to identify the subcellular location of modified or heterologous BMC-H proteins by *in vivo* fluorescent labeling of carboxysomes. We also performed a series of complementation experiments by utilizing a carboxysome-less mutant of *Syn*7942 as background strain. We showed that forming a chimeric carboxysome shell *in vivo* is possible, and changing the properties of the pores of BMC-H has no effect on assembly. Our results provide the first demonstration that pore residues are "transplantable" among shell proteins and that BMC shell proteins from different organisms and different types of carboxysomes can be combined to form chimeric shells. Given that the carboxysome and other architecturally related BMCs are promising systems for applications in synthetic biology and metabolic engineering, our work is the first step toward designing synthetic BMCs using building blocks from diverse sources.

Conserved Shell Protein Features in New High Resolution Crystal Structures of BMC-H Proteins from Both α- and β-Carboxysome. CsoS1 of *Pro9313* crystallized in space group $P2_1$ with one hexamer per asymmetric unit and diffracted to 1.9 Å resolution. CcmK2 of *Syn7942* crystallized in space group *I*2 with one hexamer in the asymmetric unit and diffracted to 2.1 Å resolution. CcmK4 of *Syn7942* crystallized in $P6_3$ space group with two monomers in the asymmetric unit; the crystallographic 3-fold symmetry generates the biological

dx.doi.org/10.1021/sb500226j | *ACS Synth. Biol.* 2015, 4, 444−453

Table 2. Data Collection and Refinement Statistics[a]

	Pro9313 CsoS1[b, c]	*Syn7942* CcmK2 [c]	*Syn7942* CcmK4 [c]
resolution range (Å)	37.3−1.90 (1.97−1.90)	36.5−2.10 (2.18−2.10)	33.7−1.34 (1.38−1.34)
space group	$P2_1$	$I2$	$P6_3$
unit cell (Å, deg)	66.2, 58.6, 81.3, 90, 113.3, 90	85.8, 73.1, 104.2, 90, 96.6, 90	67.5, 67.5, 63.4, 90, 90, 120
total reflections	167 445 (15 207)	121 163 (13 538)	319 959 (7615)
unique reflections	44 660 (4264)	31 829 (3636)	34 786 (2351)
multiplicity	3.7 (3.6)	3.7 (3.7)	9.2 (3.2)
completeness (%)	99.23 (95.47)	84.92 (93.21)	93.82 (63.42)
mean I/σ(I)	10.95 (1.86)	9.79 (2.08)	28.33 (1.63)
Wilson B-factor (Å^2)	23.57	30.15	10.93
R-merge	0.1108 (0.8135)	0.09312 (0.5774)	0.04459 (0.7226)
R-meas	0.1293	0.1088	0.04711
$CC_{1/2}$	0.988 (0.612)	0.995 (0.809)	0.999 (0.793)
R-work	0.1918 (0.3142)	0.1808 (0.2450)	0.1566 (0.3401)
R-free	0.2365 (0.3519)	0.2185 (0.3133)	0.1810 (0.3461)
no. of non-hydrogen atoms	4033	4812	1635
macromolecules	3746	4560	1453
water	287	252	182
protein residues	525	609	196
RMS (bonds)	0.007	0.004	0.020
RMS (angles)	1.08	0.84	1.80
Ramachandran favored (%)	99.8	98	98
Ramachandran outliers (%)	0	0	0
clash score	4.08	3.14	3.08
avg. B-factor	32.00	36.50	16.50
macromolecules	31.20	36.20	14.80
solvent	42.20	41.70	30.70

[a]Values in parentheses are for highest-resolution shell. [b]First single-BMC domain structure from α-cyanobacteria. [c]Model completeness: The N-terminal His6-tag used for protein purification is not visible in any of the structures. Residues that could be resolved in the electron density are Met6-Leu92 out of 103 residues for CsoS1, Pro2-Met102 out of 102 residues for CcmK2 and Met1-Arg102 out of 113 residues for CcmK4 chain A and Gln4-Pro96 for chain B.

hexamer. The CcmK4 crystals diffracted remarkably well, to 1.3 Å resolution. The structures were solved by molecular replacement and all three structures could be refined to good R/R_{free} values (19.2/23.7 for CsoS1, 18.1/21.9 for CcmK2, and 15.7/18.1 for CcmK4) and geometry with no Ramachandran outliers (data collection and refinement statistics are shown in Table 2).

All three crystal structures have the canonical BMC-H fold and hexameric quaternary structure, but they differ in crystal packing (Supporting Information (SI) Figure S1), which has been used to infer how BMC shells assemble *in vivo*.[1,3,6,33−35] CsoS1 packed in the crystal as strips of side-to-side hexamers which interact approximately orthogonally with symmetry related molecules above and below the strips (SI Figure S1). CcmK2 loosely packs as layers of concave-to-concave side facing hexamers (SI Figure S1). Those interactions between layers are mediated by residues of the short C-terminal helix, similar to the proposed dodecameric CcmK2 structure of *Thermosynechococcus elongatus*,[37] but the *Syn7942* CcmK2 hexamers are spaced about 3−4 Å further apart than in the *T. elongatus* structural model. Characterization of the hexamer−hexamer interface with PISA (Proteins, Interfaces, Structures and Assemblies)[38] suggests that the CcmK2 dodecamer is not biologically relevant (data not shown). CcmK4 also packed as layers of hexamers (Figure 1b and SI Figure S1). The buried surface area is very large (851 Å^2 per edge from each side at the interface of two adjacent hexamers; also see SI Table S1), and the packing in each CcmK4 layer is very tight (SI Table S1), reminiscent of the close packing inferred to be characteristic of the facets of the carboxysome shell *in vivo*.[1,6] This suggests that the *Syn7942* CcmK4 alone, from a structural point of view, is capable of forming the facets of the carboxysome shell just as proposed for CcmK2. This is of interest because CcmK4 has long been assumed to be only a minor component; perhaps under some growth conditions it could be the predominant building block of the carboxysome shell. In contrast, the packing observed in two crystal structures of *Synechocystis* sp. PCC 6803 CcmK4 has led to the suggestion that in general CcmK4 is not able to form homogeneous layers and is instead restricted to forming at most strips of hexameric shell proteins.[1]

Design of Chimeric Carboxysome Shell and Pore Mimics. To evaluate the potential for constructing chimeric shell facets, we modeled an α/β chimeric shell by replacing one hexamer of the *Syn7942* CcmK4 sheet with the α-carboxysome BMC-H homologue CsoS1 (Figure 1b and c). The backbone atoms align remarkably well, and none of the side chains clash, suggesting that the α-BMC-H hexamer could fit into a β-carboxysome shell. Several key residues known to form the hexamer−hexamer interface[13] are conserved (e.g., K29/K25/K26 of CsoS1A/CcmK2/CcmK4, respectively, E53/D49/D50, R83/R80/R81) while a few residues differ (e.g., E32 of CsoS1 vs R28/R29 of CcmK2/CcmK4, respectively) (Figure 1b and c). The K29/K25/K26 residue of CsoS1A/CcmK2/CcmK4, respectively, is part of a conserved D-X-X-X-K motif present on the edges of BMC-H hexamers and of each domain in BMC-T pseudohexamers, including shell proteins from metabolosomes (Figure 1a), and seems to be important for both charge and shape of hexamer−hexamer interactions.[13,34,35] The three

dx.doi.org/10.1021/sb500226j | *ACS Synth. Biol.* 2015, 4, 444−453

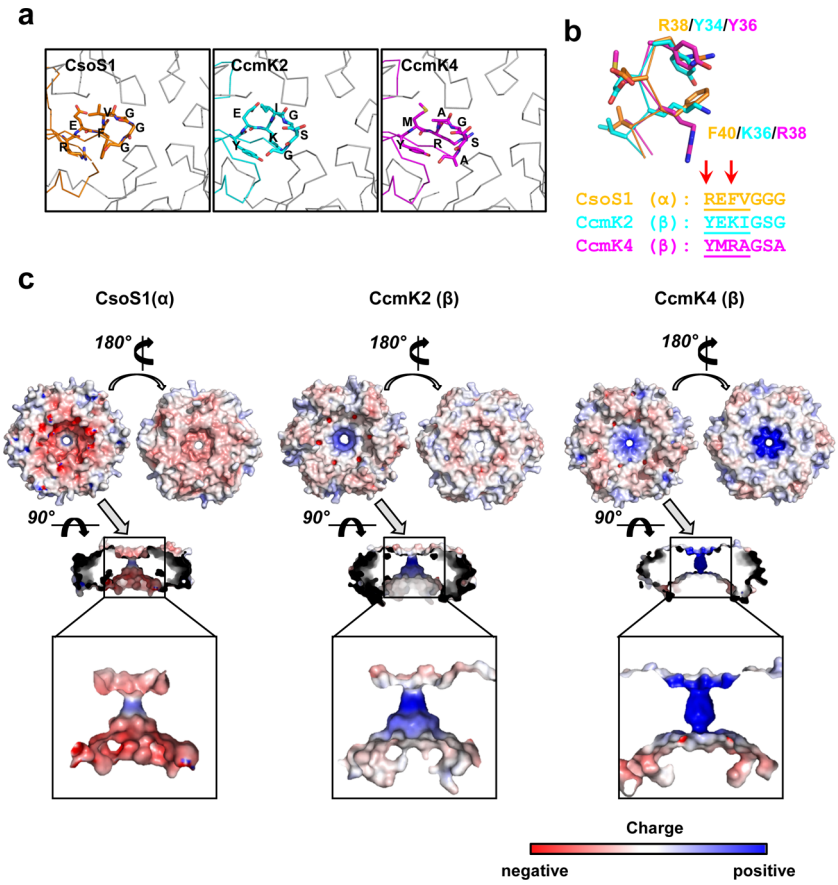

Figure 3. Structural data for the design of chimeric shell proteins. (a) Overview of pore and pore residues in the three BMC-H structures (orange, CsoS1; cyan, CcmK2; magenta, CcmK4). (b) Superposition of residues influencing pore size, shape, and charge: the CcmK proteins have an aromatic(Y/F)-X-positively charged(R/K) residue motif while CsoS1 has those properties reversed (indicated by red arrows). Residues that are substituted between CcmK2/CcmK4 and CcmK2/CsoS1 in designed pore mutants are underlined. (c) Comparison of the electrostatic potential of the CsoS1, CcmK2, and CcmK4 structures.

BMC-H structures have pores formed at the 6-fold symmetry axes of approximately the same diameter (~5 Å at the smallest constriction). However, as noted above, the conserved pore residues are different: within the β-type, CcmK2 has a conserved "K-I-G" motif flanking the pore, which is also present in other noncarboxysomal BMC-H (e.g. PduA, Figure 1a), while CcmK4 has a conserved "R-A-G" motif. CsoS1 has a glycine residue in the middle of the pore, while CcmK2 and CcmK4 proteins have a serine residue at that position (Figure 3a). Also, the residues responsible for the properties of the circumference of the pore are different between α- and β-type carboxysomes: the CcmK proteins have an aromatic(Y/F)-X-positively charged(R/K) residue motif while CsoS1 has the order of these residue types exchanged (Figure 2a and Figure 3a and b). This switch leads to different electrostatic properties inside and near the pore (Figure 3c); these are presumed to influence permeability to charged metabolites diffusing across the shell. The overall charge of CsoS1 and CcmK2/4 surfaces is also substantially different between the α- and β-carboxysome shell proteins (Figure 3c). New pore configurations were designed for both CcmK2 and CcmK4 based on these features of the three crystal structures: CcmK2$^{pm\alpha}$ (CcmK2 containing the CsoS1/α-type pore), CcmK2^{pmK4} (CcmK2 containing the CcmK4 pore), and CcmK4^{pmK2} (CcmK4 containing the CcmK2 pore).

***In Vivo* Testing of Native or Mutant BMC-H Proteins for Incorporation in β-Carboxysomes.** To test the potential for producing chimeric carboxysome shells, CsoS1, CcmK2, and CcmK4 were fused to a yellow fluorescent protein (YFP) at the C-terminus and expressed with the endogenous P_{ccmK2} promoter at *Syn7942* neutral site I (NSI) in *Syn7942* wildtype background. The resulting strains were imaged to view cellular locations of these three proteins when native β-type carboxysomes are present (Figure 4a). As previously reported,[30,36] when CcmK2 and CcmK4 proteins are labeled with a fluorescent tag in the wildtype background, carboxysomes can be visualized as spatially distributed fluorescent puncta along the long axis of the cell. By contrast, expression of YFP alone at NSI with the same promoter in the wildtype background resulted only in diffuse fluorescent signal throughout the cell (SI Figure S2). Just as in the case of CcmK2-YFP and CcmK4-YFP, a similar pattern of fluorescent puncta from CsoS1-YFP protein was also observed (Figure 4a). Although the resolution of fluorescent microscopy is not sufficient to rule out the possibility of CsoS1-YFP binding to the side of a facet (a possibility for any such shell protein fusion, e.g. in ref 36), sequence conservation and the chimeric shell model (Figure 1) suggest that edge-to-edge interactions are more robust than the face-to-face contacts observed in the crystal packing (SI Figure S1), which, even if preserved *in vivo*, would probably be disrupted by the YFP on the C-terminus. Therefore, the fluorescent pattern observed from CsoS1-YFP protein is concluded to be an indication of CsoS1 proteins incorporating into the β-carboxysome. However, this pattern is

dx.doi.org/10.1021/sb500226j | *ACS Synth. Biol.* 2015, 4, 444−453

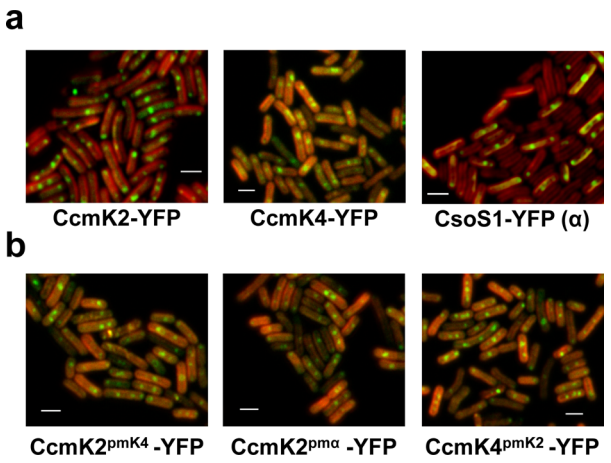

Figure 4. Cellular locations of chimeric and native BMC-H proteins in wildtype *Syn7942* carboxysomes. (a) CcmK2, CcmK4, and CsoS1 with C-terminal YFP tag; (b) three pore mutants, CcmK2$^{pm\alpha}$, CcmK2^{pmK4}, and CcmK4^{pmK2}, with C-terminal YFP tag. Bars indicate 2 μm.

not observed in all cells, which may indicate that incorporation of CsoS1 is relatively inefficient in the presence of native CcmK proteins. The level of fluorescent protein expression also varied in this strain, suggesting post-transcription and/or post-translational regulation may also influence incorporation.

We then tested the effects of transplanting pore architectures among BMC-H proteins on shell assembly, using variants of CcmK2 and CcmK4 with genetically altered pore residues designed based on crystal structures (CcmK2$^{pm\alpha}$, CcmK2^{pmK4}, and CcmK4^{pmK2}). Each mutant protein was also fused to a C-terminal YFP tag and expressed with the endogenous P_{ccmK2} promoter at NSI in a wildtype background. In all three cases, we again observed a distinct pattern of puncta (Figure 4b), similar to fluorescently labeled wildtype CcmK2 and CcmK4 (Figure 4a), suggesting that changing the properties of the pore by altering the flanking residues does not adversely affect shell protein incorporation.

Native and Pore Mutant α- and β-Type BMC-H Proteins Can Structurally Complement a CcmK2 Deletion (Carboxysome-minus) Mutant. Next, we examined the potential of the various BMC-H proteins for rescuing a carboxysome-minus mutant generated by disruption of the native CcmK2 gene. The mutant was generated by replacing the *ccmK2* open-reading frame with a kanamycin resistance cassette (Figure 5a). The *hcr* growth phenotype of this mutant, Δ*ccmK2::Kan*^{R}, is consistent with previously reported *ccmK2* gene insertion and deletion mutants[29]. However, in contrast to polar bodies formed in the *ccmK2* mutants in the same study with a diameter over 300 nm, no carboxysomes nor polar bodies are observed in our Δ*ccmK2::Kan*^{R} mutant. This morphological discrepancy between CcmK2 knockout strains might be caused by the different culturing conditions used. Moreover, it is known that a fluorescently tagged BMC-H protein cannot by itself complement a BMC-H deletion mutant;[30] the presence of additional unlabeled forms of the BMC-H protein is required. Therefore, we expressed the α- and β-type BMC-H proteins, CsoS1, CcmK2, CcmK3, and CcmK4, or the three pore mutants (CcmK2$^{pm\alpha}$, CcmK2^{pmK4}, and CcmK4^{pmK2}) individually without YFP-tag in Δ*ccmK2::Kan*^{R} background with the endogenous P_{ccmK2} promoter. Carboxysomes were observed in thin sections using transmission electron microscopy (TEM) (Figures 5b–j) for all shell proteins tested, indicating that BMC-H proteins with modified pores as well as those from the α-carboxysome can structurally rescue a carboxysome minus (Δ*ccmK2::Kan*^{R}) mutant. However, none of the resulting complementary mutants can overcome the *hcr* phenotype (data not shown). To determine if the failure to rescue *hcr* phenotype is attributable to the reduced number of carboxysomes formed (in contrast to malfunctioning ones), carboxysomes were counted in both the complemented mutants and wild type strain. A large number of cell thin sections in randomly chosen fields were sampled until a sufficient number of cells had been counted (over 300/strain), regardless of the orientation in which cells and carboxysomes were cut. These data are summarized in Table 3, revealing that carboxysomes, though formed, were present in smaller numbers in all complemented mutants compared to wildtype. Considering that the positive control (*ccmK2* gene with its native promoter) while structurally rescuing carboxysome formation likewise failed to rescue the *hcr* phenotype of Δ*ccmK2::Kan*^{R} mutant, low expression level seems the most likely cause, and consequently, the number of carboxysomes formed is not sufficient to overcome the *hcr* phenotype.

Conclusions and Outlook. Our results have important implications for both understanding the structure and function of the carboxysome as well as for bioengineering synthetic BMCs. The new crystal structures reinforce models of expected structural similarity and sequence determinants for assembly and permeability but also reveal the unexpected propensity of CcmK4 to assemble into uniformly oriented layers. CcmK4 is thought to be a minor component of the shell, but these results suggest that it could form entire shell facets; this is consistent with the experimental observation that CcmK4 can structurally complement the Δ*ccmK2::Kan*^{R} mutant. Perhaps under some growth conditions the carboxysome shell is composed predominantly of CcmK4. In terms of engineering BMCs for biotechnological applications, we demonstrated the feasibility of two different approaches to manipulating shell permeability: the construction of shell protein chimeras (in which the pore of one BMC-H paralog is mutated to mimic the pore of a different paralog) and the construction of chimeric shells. This will enable researchers to take advantage of the diversity of BMC-H shell proteins encoded in bacterial genomes as models for pore residue configurations to be introduced through genetic manipulation. Moreover, we show that it is feasible to produce chimeric shells using building blocks from diverse types of BMCs. Continuing structural and biochemical studies on BMC model systems, as well as many BMCs of unknown function, will certainly continue to enrich the toolbox for creating novel enzymatic nanoreactors.

METHODS

Protein Purification. CsoS1 from *Pro9313* was cloned into the pProEX-HTb vector (Life Technologies, Inc.) using NcoI and *Hin*dIII sites; CcmK2 and CcmK4 from *Syn*7942 were cloned into the first multiple cloning site of the pCOLA-duet vector (Novagen) using *Bam*HI and AscI sites. *E. coli* BL21 (DE3) cells were transformed with each vector. Single colonies were picked and inoculated into 200 mL LB media with 100 μg/mL ampicillin or 50 μg/mL kanamycin for pProEX-HTb and pCOLA-duet, respectively, and grown overnight at 37 °C. 6 × 1 L flasks of LB with appropriate antibiotic were inoculated with 10 mL each of saturated overnight culture and incubated at 37 °C with shaking at 200 rpm. At OD_{600} = 0.4 the temperature was lowered to 20 °C. At OD_{600} = 0.7 the cultures

dx.doi.org/10.1021/sb500226j | *ACS Synth. Biol.* 2015, 4, 444–453

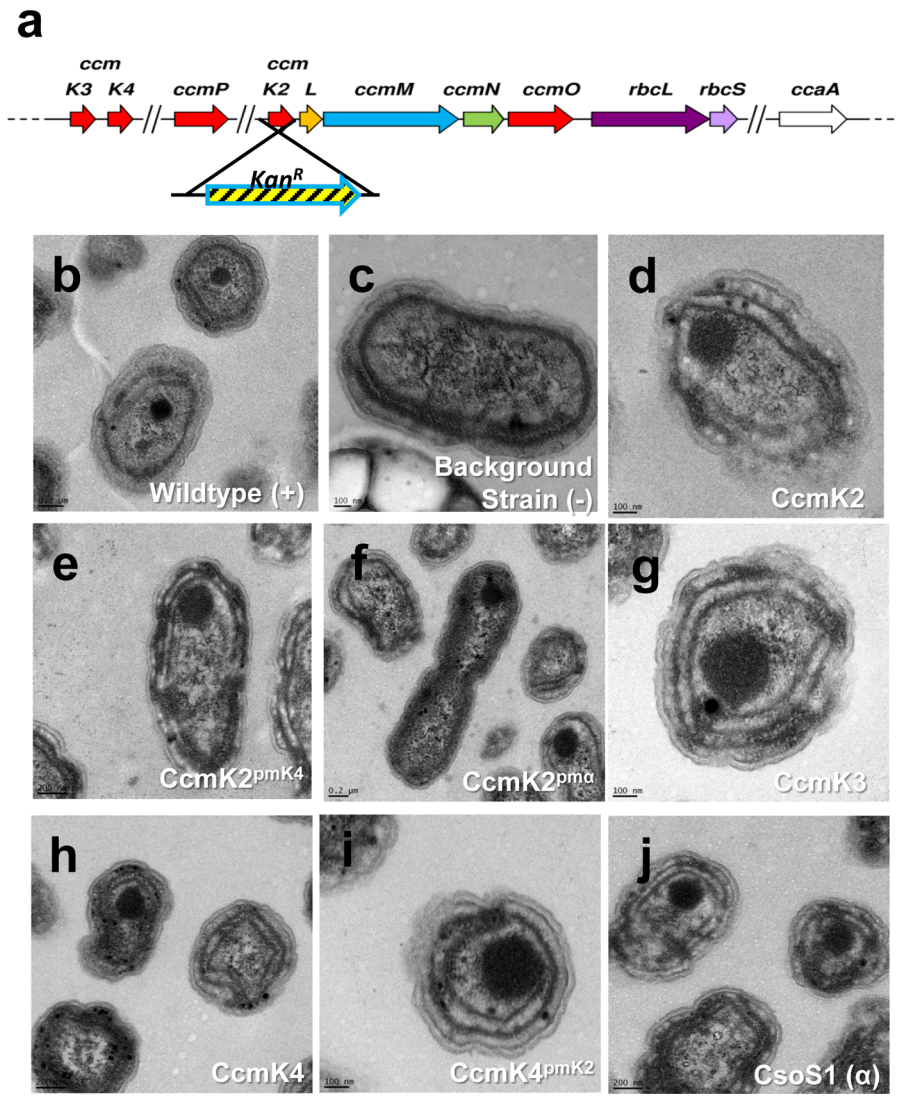

Figure 5. Structural complementation of carboxysome-less mutant. (a) Genotype of *Syn7942* Δ*ccmK2::Kan*^{R} carboxysome-minus mutant (negative control and background strain). (b–j) Transmission electron microscope images of *wildtype* and mutant *Syn7942* cells. (b) Wildtype *Syn7942* cells (positive control); (c) Δ*K2::Kan*^{R} mutant (negative control); (d) CcmK2, (g) CcmK3, (h) CcmK4, and (j) α-BMC-H protein CsoS1, expressed in Δ*K2::Kan*^{R} background; (e) pore mutants of CcmK2^{pmK4}, (f) CcmK2^{pmα}, and (i) CcmK4^{pmK2}, expressed in Δ*K2::Kan*^{R} background. Carboxysome structures are observed in all cases with the exception of the negative control. Scale bars of b, e, f, h, and j indicate 200 nm, and scale bars of c, d, g, and i indicate 100 nm.

Table 3. Carboxysomes in *Syn7942* Wildtype and Complementary Strains

sample	Csomes[a]	cell sections	Csomes/cell section	diam. (nm)[b]
wt Syn7942	121	347	0.35	207.7 ± 32.2 (100)
Δ*ccmK2::Kan*^{R}	0	230	0	N/A
Δ*ccmK2::Kan*^{R}/NS1-*Pccm_ccmK2*	20	412	0.05	211.2 ± 24.5 (20)
Δ*ccmK2::Kan*^{R}/NS1-Pccm_*ccmK2*^{pmK4}	25	479	0.05	215.6 ± 23.1 (25)
Δ*ccmK2::Kan*^{R}/NS1-Pccm_*ccmK2*^{pmα}	35	419	0.08	215.5 ± 32.7 (35)
Δ*ccmK2::Kan*^{R}/NS1-Pccm_*ccmK3*	32	325	0.10	217.6 ± 40.8 (32)
Δ*ccmK2::Kan*^{R}/NS1-Pccm_*ccmK4*	23	447	0.05	207.9 ± 23.6 (23)
Δ*ccmK2::Kan*^{R}/NS1-Pccm_*ccmK4*^{pmK2}	34	462	0.07	218.5 ± 28.1 (34)
Δ*ccmK2::Kan*^{R}/NS1-Pccm_*csoS1*	29	441	0.07	215.8 ± 26.9 (29)

[a]Csomes: short for "Carboxysomes". [b]Carboxysome diameters are the mean and standard deviation of a sample size shown in brackets.

were induced with 0.4 mM IPTG and grown overnight. Cells were harvested by centrifugation at 4000 rpm for 10 min. The pellet was resuspended in 60 mL buffer A (50 mM Tris pH 8.0, 300 mM NaCl, 1 mM β-mercaptoethanol) containing 10 mM imidazole. The suspension was sonicated for 3 min on ice using 20 s ON, 30 s OFF intervals. The lysate was then centrifuged at 15k rpm for 45 min. The supernatant was applied to Ni-NTA agarose resin and incubated by rocking at 4 °C for 1–2 h in a gravity flow column. The supernatant was decanted, and the resin washed with ~20 column volumes of buffer A containing

dx.doi.org/10.1021/sb500226j | *ACS Synth. Biol.* 2015, 4, 444–453

25 mM imidazole. The protein was eluted using buffer A containing 250 mM imidazole until no protein came off. The eluate was concentrated to 5 mg/mL and dialyzed against 10 mM Tris pH 8.0, 50 mM NaCl. The protein was loaded on S200 sephadex column for final clean up.

Crystallization. CsoS1 (5.54 mg/mL), CcmK2 (4.0 mg/mL), and CcmK4 (8.0 mg/mL) were all crystallized using a 2:1 protein/mother liquor drop ratio at room temperature. Reservoirs contained 0.1 M sodium citrate pH 5.0 with 6% (w/v) PEG 8000 (CsoS1); 0.1 M HEPES pH 6.6 with 50% (v/v) MPD (CcmK2); and 0.1 M $MgCl_2$, 0.1 M sodium citrate pH 5.0, with 15% (w/v) PEG 4000 (CcmK4). Concentrated CcmK2 also contained the short form of the encapsulation peptide from *Syn7942* CcmN[39] (VYGKEQFLRMRQSMFPDRTKVYGKEQFLRMRQSMFPD, synthesized by GenScript) at 60 μM concentration. Long CcmN C-terminal peptide[39] (EPAGRSPQSSAIAHPTKVYGKEQFLRMRQS MFPDR, synthesized by GenScript) was also added to the concentrated CcmK4 protein at 60 μM concentration before setting up the drop. Ethylene glycol (15%, w/v) was added to the drop for cryoprotection before freezing the crystals in liquid nitrogen.

Diffraction data were collected at beamline 5.0.1 of the Advanced Light Source (ALS) at Lawrence Berkeley National Lab.

Structure Determination and Analysis. Diffraction images were integrated with XDS and then scaled with SCALA (CCP4). The structures were solved using molecular replacement (Phaser in Phenix) with PDB ID 2A10. An initial model was built into the density using phenix.autosol, which was then manually corrected in Coot[40] in combination with refinement runs using phenix.refine.[41] Data collection and refinement statistics are given in Table 2.

Structural alignment using secondary structure matching followed by iterative alignment of protein C-α backbone atoms was performed with superpose in CCP4.[42] Electrostatics calculations were done with the APBS plugin for PyMOL.[43] Structure figures were prepared with PyMOL (The PyMOL Molecular Graphics System, Version 1.5.0.3 Schrödinger, LLC.)

Protein Data Bank accession codes are 4OX8 for *Pro9313* CsoS1, 4OX7 for *Syn7942* CcmK2, and 4OX6 for *Syn7942* CcmK4.

Chimeric Shell Protein Design, Pore Mutant Strains Construction, and Growth Conditions. BMC-H proteins were cloned into *Syn7942* neutral site I (NSI) vector pAM2314 with C-terminal YFP tag for cellular localization study and complementary study via standard cloning technique. Site-directed mutagenesis for three pore mutants, CcmK2$^{pm\alpha}$ (CcmK2 containing the CsoS1/α-type pore), CcmK2^{pmK4} (CcmK2 containing the CcmK4 pore), and CcmK4^{pmK2} (CcmK4 containing the CcmK2 pore), was achieved by following QuikChange Site-Directed Mutagenesis Protocol (Stratagene).

Syn7942 mutants were generated via homologous recombination as previously described[30,39]. Complete segregation of mutant strains was verified by PCR. Both *Syn7942* wildtype and mutant strains were cultured in BG-11 liquid or BG-11 agar at 30 °C under a constant illumination of ~100 microeinsteins/m^2·s in ambient or 3% CO_2 for high CO_2-requiring (*hcr*) mutants.

E. coli constructs and *Syn7942* mutant strains and primers used in this study are listed in SI Tables S2 and S3, respectively.

Fluorescence Microscopy. *Syn7942* strains expressing YFP-labeled proteins were grown in liquid culture until early log-phase (OD_{730} 1.0−2.0). Four microliters of cells were spotted on a thin BG-11 agar pad and air-dried before imaging with a Zeiss Axioplan 2 microscope or Zeiss LSM710 using a 100× oil immersion objective. Images were visualized and analyzed with ImageJ.

Transmission Electron Microscopy. Cyanobacterial cells were fixed using 2% EM-grade glutaraldehyde and 0.1 M sodium cacodylate (pH 7.2). Fixed cells were embedded in Eponate 12 resin according to standard methods. 70 nm sections were cut on a Reichert-Jung Ultracut E ultramicrotome, using a Diatome Ultra 45 diamond knife with a 6° cutting angle. Thin sections were stained with 2% methanolic uranyl acetate and then Reynolds Lead Citrate before viewing on a JEOL 1200-EX transmission electron microscope (TEM) at 80 kV. All images were taken using an Orius SC200 CCD camera.

To obtain a relatively quantitative picture of the presence of carboxysomes in the mutant and wildtype strain, carboxysomes were counted in a large number of cell thin sections in random fields of vision until a sufficient number of cells had been counted (over 300/strain, see Table 3), regardless of the orientation in which cells and carboxysomes were cut.

Phylogenetic Analysis for BMC-H Proteins. A total of 670 carboxysomal BMC-H protein sequences (65 CsoS1s and 605 CcmKs) from all 198 currently available cyanobacterial genomes, as well as the sequences of the major BMC-H protein sequences of Pdu and Eut metabolosomes (namely 35 PduA, 48 PduJ, and 13 EutM) were downloaded from the Integrated Microbial Genomes database (http://img.jgi.doe.gov). To avoid bias caused by over-representation of closely related species, redundant sequences were removed by running in-house BLASTCLUST (parameters: the sequence length to be covered was 95% and the score identity threshold was 98%). After the BLASTCLUST run, a total of 223 unique sequences (22 CsoS1s, 167 CcmKs, 15 PduA, 11 PduJ, and 8 EutM) were aligned with in-house Clustal X2[44] trimmed and submitted to PhyML (in house).[45] Maximum-likelihood trees were built with 100 bootstraps, and then visualized and edited in Dendroscope.[46] Numbers along the internodes are the percentage of instances that node was supported in 100 bootstrap replicates. HMM logos were built as described previously.[26]

■ ASSOCIATED CONTENT

Supporting Information

Figure S1: Crystal packing of the CsoS1, CcmK2 and CcmK4 structures. Figure S2: Visualization of yellow fluorescent protein (YFP) expressed in *wildtype Synechococcus elongatus* PCC 7942. Table S1: Comparison of interface between two adjacent hexamers. Table S2: Strains and plasmids used in this study. Table S3: Oligonucleotides used in cloning and segregation analysis. This material is available free of charge via the Internet at http://pubs.acs.org.

■ AUTHOR INFORMATION

Corresponding Author

*Email: ckerfeld@lbl.gov.

Author Contributions

F.C. and C.A.K. designed the experiments. F.C., M.S., S.L.B., and J.N.K. performed the experiments. F.C. and C.A.K. wrote the manuscript.

Funding

This research was supported by the NSF (MCB0851094 and MCB1160614).

Notes

The authors declare no competing financial interest.

■ ACKNOWLEDGMENTS

The Advanced Light Source is supported by the Director, Office of Science, Office of Basic Energy Sciences, of the U.S. Department of Energy under Contract No. DE-AC02-05CH11231. We thank the UC Berkeley Electron Microscopy Lab for assistance with TEM. We thank Dr. Denise Schichnes and Dr. Steven Ruzin at UC Berkeley Biological Imaging Facility for advice and assistance with fluorescent microscopy. We thank Dr. Gustaf Sandh for construction of the $\Delta K2::Kam^R$ deletion plasmid. We thank Seth Axen for preparing HMM-logos of EutM and PduA. We thank Dr. Susan Golden for providing pAM2314 vector.

■ ABBREVIATIONS

BMC, bacterial microcompartment; BMC-H, protein containing one bacterial microcompartment domain (Pfam00936); BMC-T, protein containing two bacterial microcompartment domains (Pfam00936); BMC-P, protein containing a Pfam03319 domain; CCM, CO_2-concentrating-mechanism; RubisCO, D-ribulose-1,5-bisphosphate carboxylase/oxygenase.

■ REFERENCES

(1) Kerfeld, C. A., Sawaya, M. R., Tanaka, S., Nguyen, C. V., Phillips, M., Beeby, M., and Yeates, T. O. (2005) Protein structures forming the shell of primitive bacterial organelles. *Science 309*, 936−938.

(2) Cai, F., Sutter, M., Cameron, J. C., Stanley, D. N., Kinney, J. N., and Kerfeld, C. A. (2013) The structure of CcmP, a tandem bacterial microcompartment domain protein from the β-carboxysome, forms a subcompartment within a microcompartment. *J. Biol. Chem. 288*, 16055−16063.

(3) Takenoya, M., Nikolakakis, K., and Sagermann, M. (2010) Crystallographic insights into the pore structures and mechanisms of the EutL and EutM shell proteins of the ethanolamine-utilizing microcompartment of *Escherichia coli*. *J. Bacteriol. 192*, 6056−6063.

(4) Klein, M. G., Zwart, P., Bagby, S. C., Cai, F., Chisholm, S. W., Heinhorst, S., Cannon, G. C., and Kerfeld, C. A. (2009) Identification and structural analysis of a novel carboxysome shell protein with implications for metabolite transport. *J. Mol. Biol. 392*, 319−333.

(5) Tanaka, S., Kerfeld, C. A., Sawaya, M. R., Cai, F., Heinhorst, S., Cannon, G. C., and Yeates, T. O. (2008) Atomic-level models of the bacterial carboxysome shell. *Science 319*, 1083−1086.

(6) Tsai, Y., Sawaya, M. R., Cannon, G. C., Cai, F., Williams, E. B., Heinhorst, S., Kerfeld, C. A., and Yeates, T. O. (2007) Structural analysis of CsoS1A and the protein shell of the *Halothiobacillus neapolitanus* carboxysome. *PLoS Biol. 5*, e144.

(7) Cai, F., Menon, B. B., Cannon, G. C., Curry, K. J., Shively, J. M., and Heinhorst, S. (2009) The pentameric vertex proteins are necessary for the icosahedral carboxysome shell to function as a CO_2 leakage barrier. *PLoS One 4*, e7521.

(8) Jorda, J., Lopez, D., Wheatley, N. M., and Yeates, T. O. (2013) Using comparative genomics to uncover new kinds of protein-based metabolic organelles in bacteria. *Protein Sci. 22*, 179−195.

(9) Kerfeld, C. A., Heinhorst, S., and Cannon, G. C. (2010) Bacterial microcompartments. *Annu. Rev. Microbiol. 64*, 391−408.

(10) Beeby, M., Bobik, T. A., and Yeates, T. O. (2009) Exploiting genomic patterns to discover new supramolecular protein assemblies. *Protein Sci. 18*, 69−79.

(11) Erbilgin, O., McDonald, K. L., and Kerfeld, C. A. (2014) Characterization of a planctomycetal organelle: A novel bacterial microcompartment for the aerobic degradation of plant saccharides. *Appl. Environ. Microbiol. 80*, 2193−2205.

(12) Petit, E., LaTouf, W. G., Coppi, M. V., Warnick, T. A., Currie, D., Romashko, I., Deshpande, S., Haas, K., Alvelo-Maurosa, J. G., Wardman, C., Schnell, D. J., Leschine, S. B., and Blanchard, J. L. (2013) Involvement of a bacterial microcompartment in the metabolism of fucose and rhamnose by *Clostridium phytofermentans*. *PLoS One 8*, e54337.

(13) Kinney, J. N., Axen, S. D., and Kerfeld, C. A. (2011) Comparative analysis of carboxysome shell proteins. *Photosynth Res. 109*, 21−32.

(14) Yeates, T. O., Jorda, J., and Bobik, T. A. (2013) The shells of BMC-type microcompartment organelles in bacteria. *J. Mol. Microbiol. Biotechnol. 23*, 290−299.

(15) Frank, S., Lawrence, A. D., Prentice, M. B., and Warren, M. J. (2013) Bacterial microcompartments moving into a synthetic biological world. *J. Biotechnol. 163*, 273−279.

(16) Kim, E. Y., and Tullman-Ercek, D. (2013) Engineering nanoscale protein compartments for synthetic organelles. *Curr. Opin. Biotechnol. 24*, 627−632.

(17) Zarzycki, J., Axen, S. D., Kinney, J. N., and Kerfeld, C. A. (2013) Cyanobacterial-based approaches to improving photosynthesis in plants. *J. Exp. Bot. 64*, 787−798.

(18) Lassila, J. K., Bernstein, S. L., Kinney, J. N., Axen, S. D., and Kerfeld, C. A. (2014) Assembly of robust bacterial microcompartment shells using building blocks from an organelle of unknown function. *J. Mol. Biol. 426*, 2217.

(19) Howorka, S. (2011) Rationally engineering natural protein assemblies in nanobiotechnology. *Curr. Opin. Biotechnol 22*, 485−491.

(20) Doll, T. A., Raman, S., Dey, R., and Burkhard, P. (2013) Nanoscale assemblies and their biomedical applications. *J. R. Soc. Interface 10*, 20120740.

(21) Agapakis, C. M., Boyle, P. M., and Silver, P. A. (2012) Natural strategies for the spatial optimization of metabolism in synthetic biology. *Nat. Chem. Biol. 8*, 527−535.

(22) Chen, A. H., and Silver, P. A. (2012) Designing biological compartmentalization. *Trends Cell Biol. 22*, 662−670.

(23) Price, G. D., Pengelly, J. J., Forster, B., Du, J., Whitney, S. M., von Caemmerer, S., Badger, M. R., Howitt, S. M., and Evans, J. R. (2013) The cyanobacterial CCM as a source of genes for improving photosynthetic CO_2 fixation in crop species. *J. Exp Bot 64*, 753−768.

(24) Lawrence, A. D., Frank, S., Newnham, S., Lee, M. J., Brown, I. R., Xue, W., Rowe, M. L., Mulvihill, D. P., Prentice, M. B., Howard, M. J., and Warren, M. J. (2014) Solution structure of a bacterial microcompartment targeting peptide and its application in the construction of an ethanol bioreactor. *ACS Synth. Biol. 30*, 2014 DOI: 10.1021/sb4001118.

(25) Roberts, E. W., Cai, F., Kerfeld, C. A., Cannon, G. C., and Heinhorst, S. (2012) Isolation and characterization of the *Prochlorococcus carboxysome* reveal the presence of the novel shell protein CsoS1D. *J. Bacteriol. 194*, 787−795.

(26) Cai, F., Kerfeld, C. A., and Sandh, G. (2012) Bioinformatic identification and structural characterization of a new carboxysome shell protein. *Adv. Photosynth. Respir. 33*, 12.

(27) Schwarz, D., Nodop, A., Huge, J., Purfurst, S., Forchhammer, K., Michel, K. P., Bauwe, H., Kopka, J., and Hagemann, M. (2011) Metabolic and transcriptomic phenotyping of inorganic carbon acclimation in the cyanobacterium *Synechococcus elongatus* PCC 7942. *Plant Physiol. 155*, 1640−1655.

(28) Vijayan, V., Jain, I. H., and O'Shea, E. K. (2011) A high resolution map of a cyanobacterial transcriptome. *Genome Biol. 12*, R47.

(29) Rae, B. D., Long, B. M., Badger, M. R., and Price, G. D. (2012) Structural determinants of the outer shell of β-carboxysomes in *Synechococcus elongatus* PCC 7942: Roles for CcmK2, K3-K4, CcmO, and CcmL. *PLoS One 7*, e43871.

(30) Cameron, J. C., Wilson, S. C., Bernstein, S. L., and Kerfeld, C. A. (2013) Biogenesis of a bacterial organelle: The carboxysome assembly pathway. *Cell 155*, 1131−1140.

(31) Tanaka, S., Sawaya, M. R., and Yeates, T. O. (2010) Structure and mechanisms of a protein-based organelle in *Escherichia coli*. *Science 327*, 81−84.
(32) Pitts, A. C., Tuck, L. R., Faulds-Pain, A., Lewis, R. J., and Marles-Wright, J. (2012) Structural insight into the *Clostridium difficile* ethanolamine utilisation microcompartment. *PLoS One 7*, e48360.
(33) Crowley, C. S., Cascio, D., Sawaya, M. R., Kopstein, J. S., Bobik, T. A., and Yeates, T. O. (2010) Structural insight into the mechanisms of transport across the *Salmonella enterica* Pdu microcompartment shell. *J. Biol. Chem. 285*, 37838−37846.
(34) Sinha, S., Cheng, S., Sung, Y. W., McNamara, D. E., Sawaya, M. R., Yeates, T. O., and Bobik, T. A. (2014) Alanine scanning mutagenesis identifies an asparagine-arginine-lysine triad essential to assembly of the shell of the pdu microcompartment. *J. Mol. Biol. 426*, 2328−2345.
(35) Pang, A., Frank, S., Brown, I., Warren, M. J., and Pickersgill, R. W. (2014) Structural insights into higher-order assembly and function of the bacterial microcompartment protein PduA. *J. Biol. Chem. 289*, 22377.
(36) Savage, D. F., Afonso, B., Chen, A. H., and Silver, P. A. (2010) Spatially ordered dynamics of the bacterial carbon fixation machinery. *Science 327*, 1258−1261.
(37) Samborska, B., and Kimber, M. S. (2012) A dodecameric CcmK2 structure suggests β-carboxysomal shell facets have a double-layered organization. *Structure 20*, 1353−1362.
(38) Krissinel, E., and Henrick, K. (2007) Inference of macromolecular assemblies from crystalline state. *J. Mol. Biol. 372*, 774−797.
(39) Kinney, J. N., Salmeen, A., Cai, F., and Kerfeld, C. A. (2012) Elucidating essential role of conserved carboxysomal protein CcmN reveals common feature of bacterial microcompartment assembly. *J. Biol. Chem. 287*, 17729−17736.
(40) Emsley, P., and Cowtan, K. (2004) Coot: Model-building tools for molecular graphics. *Acta Crystallogr. D Biol. Crystallogr. 60*, 2126−2132.
(41) Afonine, P. V., Grosse-Kunstleve, R. W., Echols, N., Headd, J. J., Moriarty, N. W., Mustyakimov, M., Terwilliger, T. C., Urzhumtsev, A., Zwart, P. H., and Adams, P. D. (2012) Towards automated crystallographic structure refinement with phenix.refine. *Acta Crystallogr., Sect. D: Biol. Crystallogr. 68*, 352−367.
(42) Winn, M. D., Ballard, C. C., Cowtan, K. D., Dodson, E. J., Emsley, P., Evans, P. R., Keegan, R. M., Krissinel, E. B., Leslie, A. G., McCoy, A., McNicholas, S. J., Murshudov, G. N., Pannu, N. S., Potterton, E. A., Powell, H. R., Read, R. J., Vagin, A., and Wilson, K. S. (2011) Overview of the CCP4 suite and current developments. *Acta Crystallogr., Sect. D: Biol. Crystallogr. 67*, 235−242.
(43) Baker, N. A., Sept, D., Joseph, S., Holst, M. J., and McCammon, J. A. (2001) Electrostatics of nanosystems: Application to microtubules and the ribosome. *Proc. Natl. Acad. Sci. U.S.A. 98*, 10037−10041.
(44) Larkin, M. A., Blackshields, G., Brown, N. P., Chenna, R., McGettigan, P. A., McWilliam, H., Valentin, F., Wallace, I. M., Wilm, A., Lopez, R., Thompson, J. D., Gibson, T. J., and Higgins, D. G. (2007) Clustal W and Clustal X version 2.0. *Bioinformatics 23*, 2947−2948.
(45) Dereeper, A., Guignon, V., Blanc, G., Audic, S., Buffet, S., Chevenet, F., Dufayard, J. F., Guindon, S., Lefort, V., Lescot, M., Claverie, J. M., and Gascuel, O. (2008) Phylogeny.fr: Robust phylogenetic analysis for the non-specialist. *Nucleic Acids Res. 36*, W465−469.
(46) Huson, D. H., Richter, D. C., Rausch, C., Dezulian, T., Franz, M., and Rupp, R. (2007) Dendroscope: An interactive viewer for large phylogenetic trees. *BMC Bioinformatics 8*, 460.
(47) Edgar, R. C. (2004) MUSCLE: Multiple sequence alignment with high accuracy and high throughput. *Nucleic Acids Res. 32*, 1792−1797.
(48) Eddy, S. R. (1998) Profile hidden Markov models. *Bioinformatics 14*, 755−763.
(49) Schuster-Bockler, B., Schultz, J., and Rahmann, S. (2004) HMM Logos for visualization of protein families. *BMC Bioinformatics 5*, 7.